CHAPTER IV

TROPICAL ATMOSPHERIC BOUNDARY LAYER: OBSERVATIONS

This chapter discusses the observations of the development of the planetary boundary layer in the tropics. In addition, the location, climatology of the site, data collection, and instrumentation used in the measurements are discussed.

Due to the lack of detailed observations in the near-equatorial region, the Tropical Boundary Layer Experiments (TBLEs) during the Northeast and Southwest monsoons were conceived to collect data on the evolution of the tropical ABL. Of particular interest are specific features of the tropical atmospheric boundary layer related to turbulent and radiative characteristics in the presence of buoyancy. The intention is to observe the evolution of the boundary layer both during convective and stable situations.

The main observations of the Tropical Boundary Layer Experiments (TBLEs), which were collected during the months of January and September 2000 at the University of Malaya campus, are presented. The ABL is analysed using radiosonde measurements, to characterise the diurnal and nocturnal evolution of the

tropical boundary layer. Using the two data sets, a mean composite of virtual potential temperature during convective and stable conditions is derived.

This chapter deals with the observations of the PBL growth and decay observed during the TBLEs. A companion analysis (Chapter VI) will describe some of the modelling aspects of the experiments.

4.1 EXPERIMENTAL LOCATION

In accordance with the stated goal, the TBLEs were conceived to collect conventional radiosonding with detailed profiles at the campus of the University of Malaya. The launch site is at 3.12' N and 101.65' E at an altitude of 46 m above the mean sea level, and lies 50 km inland from the west coast.

Figure 4.1 depicts the geographic location of Klang Valley region including the location of the experimental site. The Klang Valley region is a highly populated and industrialised urban area. This region includes *Kuala Lumpur*, the capital city of Malaysia; *Petaling Jaya*, a densely populated and industrialised area; *Shah Alam*, the state capital; and *Klang* and *Port Klang*.

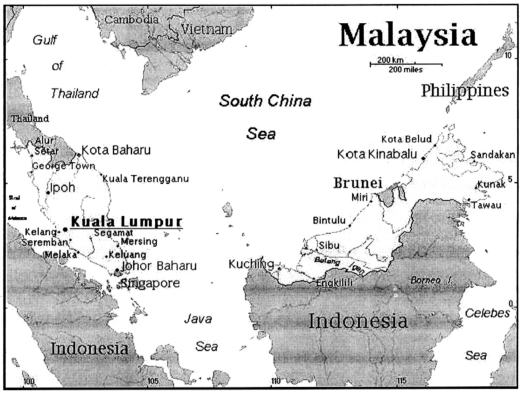

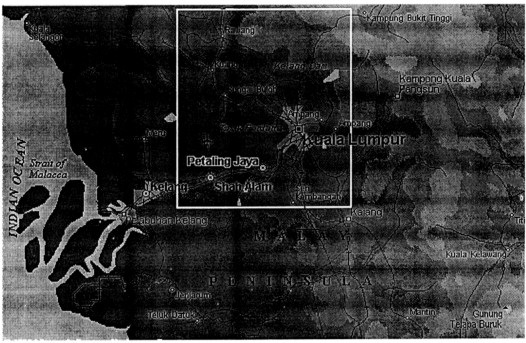

Figure 4.1.: Geographic location of the experimental site, Petaling Jaya, Malaysia.

4.2 DATA COLLECTION AND INSTRUMENTATION

4.2.1 Observations and Instrumentation

Atmospheric boundary layer data were taken using a slow rise radiosonde with an ascent velocity of about 3 m/s. A four-hourly ascent schedule was made during cloudy days, with an intensive two-hourly ascent schedule being made during clear days. Sondes were launched at 8:00, (10:00), 12:00, (14:00), 16:00, (18:00), 20:00, 22:00 and 24:00 local time (LT), where times in parentheses indicate extra soundings during cloud-free days. The sonde data measured temperature, wet bulb temperature, pressure, wind speed, and wind direction. These data were subsequently used to calculate the virtual potential temperature and mixing ratio profiles.

The soundings were collected using a Vaisala (Finland) radiosounding system, the RS80-15G radio-sounder. These sondes measure air temperature (Thermistor - THERMOCAP), relative humidity (electronic capacitor - HUMICAP) and atmospheric pressure (Barometric capsule - BAROCAP), which, when launched into the atmosphere, emits signals at a sampling rate of 0.5 Hz. The raw sondes data were then changed to a text file in which a ten-second interval was selected. This file was then used to calculate the thermodynamic parameters such as potential temperature, virtual potential temperature, equivalent potential temperature, and mixing ratio. Information on wind (direction and speed) was obtained through the localised GPS system that permits soundings every 3 seconds.

The radiosondes were flown using 100 g meteorological balloons, which have a slow mean ascension rate of about 3 m/s. Before launching, the radiosonde was calibrated with values measured at the surface by independent instruments: a psychrometer for air temperature and relative humidity; a barometer for atmospheric pressure; and an anemometer for wind direction and speed. Normally, the radiosonde reached an altitude higher than 20 km, although, in this study, only values measured up to 5 km altitude were used. During the TBLE experiments, the receiver used was the portable Vaisala MARWIN MW 12 DIGICORA set which is factory calibrated. The balloons burst at altitude of 15-20 km.

According to the manufacturer, the temperature sensor resolution is 0.1 °C, the humidity sensor resolution is 1 %, and the pressure sensor resolution is 0.1 hPa. For the wind determination, the manufacturer calibration is 0.5 m/s for the speed resolution and 1 degree for the wind direction resolution.

For the studies of the boundary layer's temporal evolution, not only were profile data necessary but also complementary data of turbulent fluxes (momentum, sensible and latent heat) at the surface; routine meteorological observations were also recorded.

4.2.2 Climatology of the Experimental Site (Klang-Valley)

Generally, there are four seasons in Malaysia based on the periodic changes in the wind flow pattern. These are the Southwest (SW) monsoon, the Northeast (NE) monsoon, and two intermonsoons. The SW monsoon lasts from June to September,

the NE monsoon from December to March, and the intermonsoon months are from April to May and October to November (Lim & Leong, 1991; Zainal Abidin, 1993).

The climatology of the Klang Valley region is now discussed briefly, using conventional meteorological data measured at the Malaysian Meteorological Service (MMS) climatic station located in Petaling Jaya (PJ). The data set has been provided by the MMS. The PJ station is about 3 km to the west of the launching site (UM-campus). Hence, it represents a good representation of the general conditions at the site.

Figures 4.2 and 4.3 present the climatological patterns of air temperature and rainfall respectively for the PJ area. Monthly average values are available from 1990 until 1999. They were analysed in order to give general characteristics of the region. Monthly average values indicate a strong seasonality in rainfall (Figure 4.2). During the dry period the monthly precipitation is less than 200 mm, while it reaches values in excess of 350 mm during the wet period. As for the air temperature (Figure 4.3), the data show that the mean air temperature is at a maximum around June of 28 °C and a minimum around December of 26.5 °C.

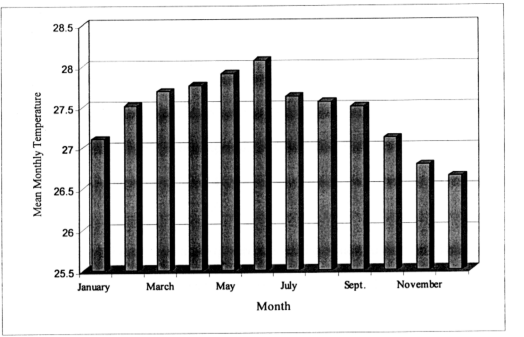

Figure 4.2: Representative pattern of temperature (°C) for the experimental site, 1990-1999 (source: Malaysian Meteorological Services).

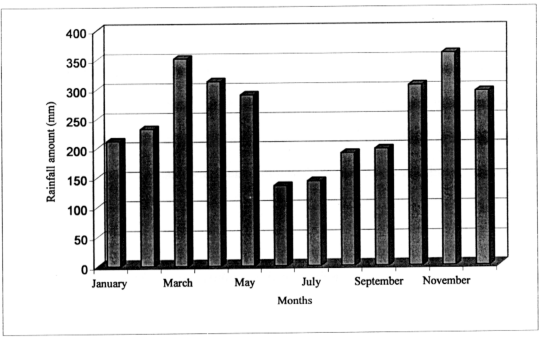

Figure 4.3: Representative pattern of rainfall amount (mm) for the experimental site, 1990-1999 (source: Malaysian Meteorological Services).

4.3 TROPICAL BOUNDARY LAYER EXPERIMENTS (TBLES)

The TBLEs had two distinct data collection missions: TBLE during the NE monsoon (NE-TBLE) and during the SW Monsoon (SW-TBLE) in the year 2000. The NE-TBLE campaign took place between January 24th and 30th, and the SW-TBLE was executed from September 11th to 14th.

To determine the main characteristics of the structure of the ABL during the TBLEs, a composite profile was made for each experiment. For the NE-TBLE, 7 days were used in the analysis, and 4 days in the SW-TBLE analysis.

4.3.1 Tropical Boundary Layer Experiment During The North-East Monsoon (NE-TBLE)

Using a slow rise radiosonde ascent, a four-hourly observation schedule was used for cloudy conditions and a two-hourly observation schedule during clear days, and used in the analysis below. The cloudy days were 26th, 28th, 29th and 30th of January 2000, while the day of 27^{th,} January was a clear day with the intensive two-hourly interval ascents.

4.3.1.1 NE-TBLE Micrometeorological Description

To characterise the weather patterns during the TBLE, an average hourly time series of the global solar energy, temperature, wind speed, and wind direction are

presented. Figures 4.4a, b, c, and d show the behaviour of those parameters during the NE-TBLE.

Figure 4.4a shows the solar radiation variation during the period of the experiment. The diurnal cycle is well characterised. The maximum radiation observed was for the 27th of January which was a clear, sunny day. Air temperature values showed a similar behaviour with higher values of 32 ^{o}C in the afternoon on the 26th, 27th and 28th (Figure 4.4b). For the relative humidity measurements, only the daily values are presented and the pattern shows low values on the 27th compared to the other days of the experiment. Similarly, the wind speed also exhibited a distinct diurnal cycle (Figure 4.4c), with speeds of 3 m/s during the afternoon when turbulence is at its maximum. At night, the wind was essentially calm (less than 0.5 m/s). The wind direction was variable during the whole experiment (Figure 4.4d).

The weather was dry for almost the entire observation period, with no rainfall except on the 24th when a short burst of afternoon shower occurred in which 18.2 mm of rainfall was recorded.

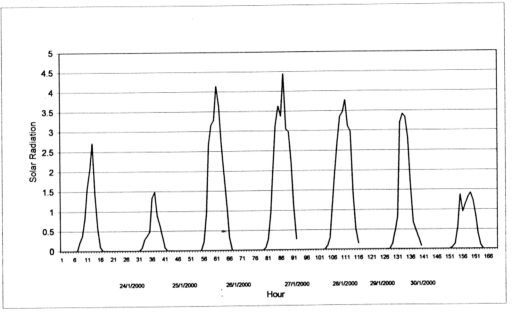

Figure 4.4 a: Time series of the hourly values of solar radiation during NE-TBLE.

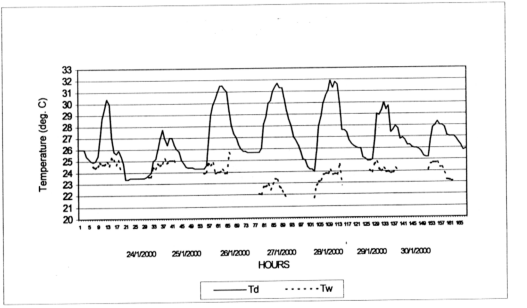

Figure 4.4 b: Time series of the hourly values of temperature during NE-TBLE.

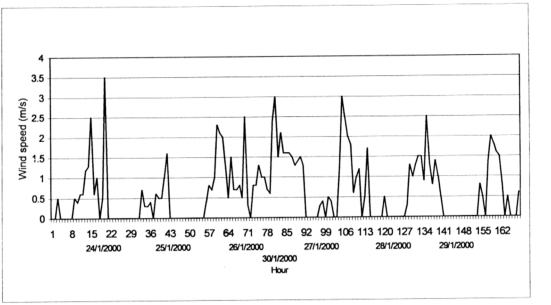

Figure 4.4 c: Time series of the hourly values of wind speed during NE-TBLE.

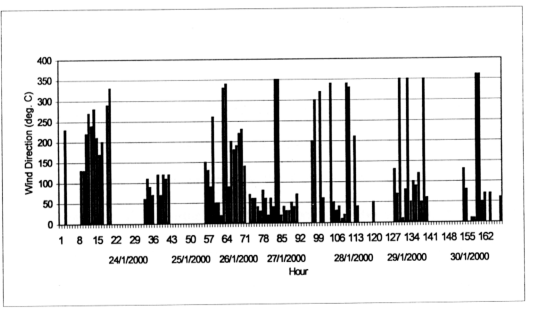

Figure 4.4 d: Time series of the hourly values of wind direction during NE-TBLE.

4.3.1.2 Observations of the Convective Boundary Layer Evolution during the NE-TBLE

In this section the structure and evolution of the CBL height growth under different conditions are discussed. The evolution of the boundary layer is demonstrated by using thermodynamic properties such as virtual potential temperature, potential temperature, and the mixing ratio. The CBL growth is further sub-categorised into clear and cloudy days.

The characterisation of the CBL height is far simpler than the nocturnal one, because the θv is well mixed within the TABL (due to the thermal convection and mechanical turbulence), showing a well-marked inflection at the top of the TABL. The mixing layer height was determined by visual inspection of the virtual potential temperature profile, at the point of inflection.

The analysis of the CBL was categorised into clear and cloudy days, in order to investigate any differences that might arise due to the effect of cloud and associated processes that might modify the CBL. In the case of cloudy days, individual profiles of the virtual potential temperature (θv) were determined and linearly interpolated at 50 m intervals. There profiles were grouped as a function of local time and the mean profile was a composite of all the respective cloudy days observed. A typical mean profile was obtained for each local time for which soundings data were available. For the composite, the growth rate (m/h) of the CBL was determined from the height variation with elapsed time, and the heating rate was

determined from the temporal variation of the mean virtual potential temperature of the mixing layer (K/h) (Fisch, 1996).

The Convective Boundary Layer Evolution on a Clear Day

The observations of the CBL by radiosonding were made at the times of 8:00, 10:00, 12:00, 14:00, 16:00, and 18:00 LT, on the clear day (27th January). Table 4.1 presents data measured at these times for the evolution of the CBL height (h_c), the mean virtual potential temperature (θ_v) of the mixing layer, and the gradient of virtual potential temperature above the CBL top (γ_o).

From Table 4.1, it can be seen that the initial depth was 150 m at 8:00 LT. The CBL height increased rapidly to 1450 m by about 10:00 LT with a growth rate of 650 m/h. After this, a slower growth rate of 150 m/h was observed. The mixed layer had reached a height of 1750 m by midday (12:00 LT). Later in the afternoon, the mixed layer was observed to be well developed and well mixed with a CBL of 1600 m at 14:00 LT. A second growth was observed to occur increasing the height to the highest value of the day of 2700 m at 16:00 LT. The growth rate of this second period was estimated to be in the order of 550 m/h. The boundary layer height was observed to drop in the evening, at a rate of -225 m/h, to reach 2250 m at 18:00 LT. The virtual potential temperature gradient above the inversion (the CBL top) also showed temporal variations, beginning with 3.84 K/km at 8:00 and progressively increasing to 7.6 K/km at 16:00 LT (Table 4.1). Figures 4.5a-f show the vertical profiles of the virtual temperature at times of 8:00, 10:00, 12:00, 14:00, 16:00 and 18:00 LT respectively.

Table 4.1: Values of the height of the boundary layer (h_c), of the mean virtual potential temperature (θ_v) of the CBL, and of the gradient of virtual potential temperature above the top of the CBL (S_0) in diurnal conditions observed during a clear day of the NE-TBLE (27th January 2000).

Local Time	CBL height (m)	θ_v (K)	S_0 (K/km)
8:00	150	300.45	3.84
10:00	1450	303.25	5.43
12:00	1750	305.15	5.67
14:00	1600	305.45	5.46
16:00	2700	307.05	7.6
18:00	2250	306.7	6

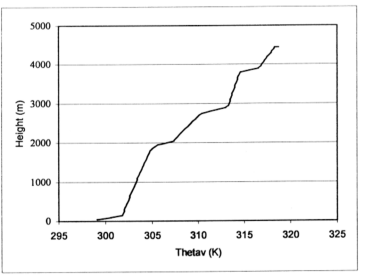

Figure 4. 5a: Vertical profile of the virtual potential temperature at 8:00 LT (27th January 2000).

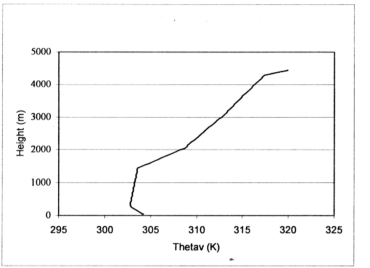

Figure 4.5b: Vertical profile of the virtual potential temperature at 10:00 LT (27th January 2000).

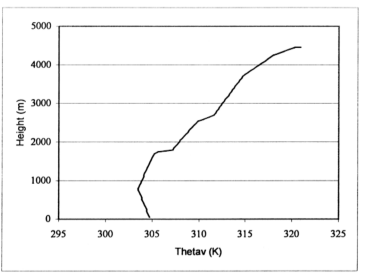

Figure 4. 5c: Vertical profile of the virtual potential temperature at 12:00 LT (27th January 2000).

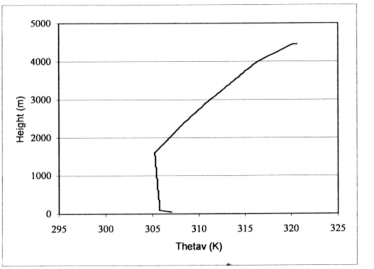

Figure 4.5d: Vertical profile of the virtual potential temperature at 14:00 LT (27th January 2000).

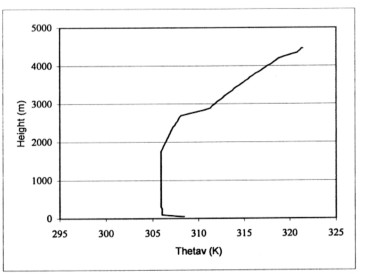

Figure 4.5e: Vertical profile of the virtual potential temperature at 16:00 LT (27th January 2000).

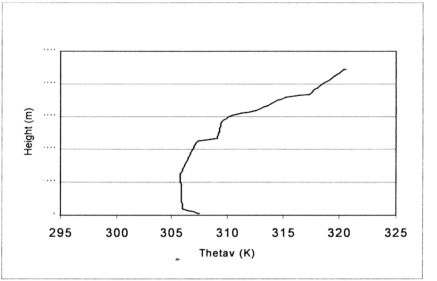

Figure 4.5f: Vertical profile of the virtual potential temperature at 18:00 LT (27th January 2000).

The behaviour of the mixed layer mean virtual potential temperature is coherent with the diurnal cycle, beginning with a value of 300.45 K and reaching a maximum temperature of 307.05 K at 16:00 LT, later decreasing to 306.7 K in the evening (18:00 LT). Figure 4.5g shows the hourly variation of the mixing layer mean temperature for 27th January. The heating rate was higher in the early part of the morning (1.4 K/h) when the surface heating eroded the stable nocturnal layer. Subsequently, there was slow heating with a heating rate of 0.95 K/h till midday and the rate further decreased to 0.15 K/h at 14:00 LT. The heating rate was observed to increase and stabilise to 0.8 K/h between 14:00 and 16:00 LT. During the afternoon, the surface sensible heat flux began to decrease, but the layer as a whole maintained (or slowly increased) its temperature. This could be due to the role of entrainment flux that entrained drier and cooler air above the CBL. The entrained flux is of the same order as the surface heat flux, which can be evaluated by performing a simple

estimation with the energy conservation equation in the layer. In the evening, due to radiational cooling, the layer started to cool at a rate of -0.175 K/h from 18:00 LT.

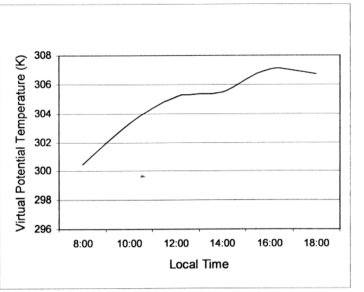

Figure 4.5g: The hourly variations of the mixing layer mean temperature on 27th January 2000.

The Convective Boundary Layer Evolution on a Cloudy Day

Composite profiles of the virtual potential temperature for the cloudy days of 26th, 28th, and 29th January were used in the analysis and characterisation of the evolution of the CBL for a "typical" cloudy day. Table 4.2 presents values for the CBL height (hc), the mean virtual potential temperature (θ_v) of the mixing layer, and the gradient of virtual potential temperature above the CBL top (γ_θ), during cloudy conditions.

In the initial stage, the CBL was around 300 m at 8:00 LT, with a mean virtual potential temperature of 300.27 K. The mixed layer height increased rapidly reaching the values of 1800 m at 12:00 LT and 2050 m at 16:00 LT. The growth rate

was high during the first hours of the morning at 375 m/h, decreasing to 62.5 m/h between 12:00 and 16:00 LT. The mean potential virtual temperature of the mixed layer was observed to increase rapidly from 300.27 K to 305.19 K between 8:00 and 12:00 LT, resulting in a heating rate of 1.23 K/h. After 12:00 LT, the heating rate decreased to 0.365 K/h between 12:00 LT and 16:00 LT. The mean virtual potential temperature at 16:00 LT had a value of 306.65 K. The maximum growth rate was observed during 8:00 LT and 12:00 LT when the nocturnal boundary layer was already eroded, the surface energy fluxes were at their maximum values, and the heating rate was greatest. The virtual potential temperature gradient of the CBL top also exhibited temporal variations, varying from 4.31 K/km in the morning to 5.36 K/km in the afternoon (Table 4.2). Figures 4.6a-c display the vertical profile of the virtual potential temperature observed on cloudy days during the NE-TBLE.

Table 4.2: Values of the height of the boundary layer (h_c), of the mean virtual potential temperature (θ_v) of the CBL and of the gradient of virtual potential temperature above the top of the CBL (γ_θ) under diurnal cloudy conditions observed during NE-TBLE (26th, 28th and 29th January 2000).

Local Time	**CBL height (m)**	θ_v **(K)**	γ_θ **(K/km)**
8:00	300	300.27	4.31
12:00	1800	305.19	5.3
16:00	2050	306.65	5.36

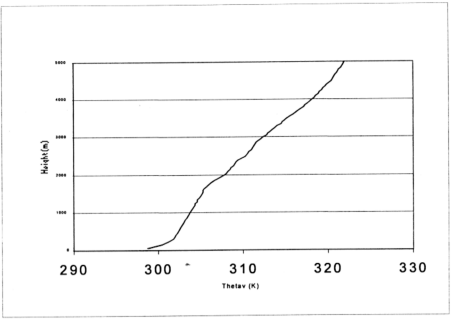

Figure 4.6a: Composite vertical profile of the virtual potential temperature at 8:00 LT (26th, 28th, and 29th January 2000).

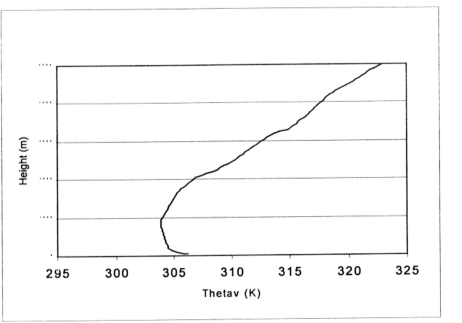

Figure 4.6b: Composite vertical profile of the virtual potential temperature at 12:00 LT (26th, 28th, and 29th January 2000).

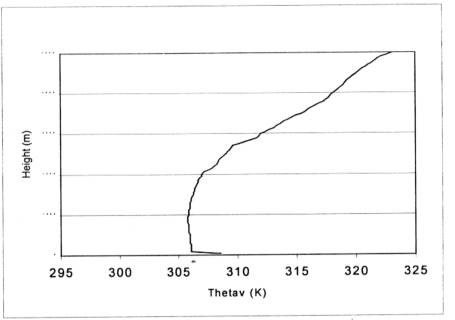

Figure 4.6c: Composite vertical profile of the virtual potential temperature at 16:00 LT (26th, 28th, and 29th January 2000).

4.3.1.3 Nocturnal Boundary Layer Evolution during the NE-TBLE

As revealed in the literature, there is a variety of methods used for the estimation of the height of the nocturnal boundary layer (NBL) top. The most frequently used criteria are the height at which the virtual potential temperature (θ_v) gradient turns to zero or when there is a cessation of turbulence (Stull, 1988). These criteria are summarised by Beyrich & Weill (1993) who associated them with dynamic characteristics (associated with winds in the NBL), thermal characteristics (associated with the θv profile), and turbulence (associated with turbulent fluxes). However, for a given vertical profile and depending on the method used, the estimated NBL height will be different (Garratt, 1992).

In this study, the chosen method was to define the top of the NBL as being the height where the θv vertical gradient is null or very small. This definition of the height of the NBL considers the maximum distance from the surface where the nocturnal cooling acts (Nieuwstadt, 1980).

In order to determine the main characteristics of the NBLs during the NE-TBLE, the virtual potential temperature profiles of the days 26th through 29th January were used. The ascents were made at the following times: 20:00, 24:00, 4:00, and 6:00 LT. The profile for 20:00 was calculated with two releases while the profiles for 24:00, 4:00, and 6:00 LT were calculated with 3 releases. The profiles were interpolated at an interval of 50 m and grouped as a function of hours. Subsequently, a mean profile was calculated for every time period and the mean characteristics determined as a function of this profile.

The nocturnal boundary layer characteristics measured during the NE-TBLE were the boundary layer heights (h_s), the virtual potential temperature (θ_v (h_s)) at the top of the layer, and the thermal inversion discontinuity ($\Delta\theta_v$), values of which are reported in Table 4.3.

In the following analysis, the thermal discontinuity (K), is defined as the difference between the virtual potential temperature at the top of the nocturnal boundary layer and the surface. The intensity of the thermal inversion (K/km) is defined as the thermal discontinuity divided by the thickness of the layer. The layer cooling rate (K/h) is estimated by the temporal variation of the virtual potential temperature at the top of the NBL (Fisch, 1996).

At 20:00 LT, the profile does not indicate the development of nocturnal boundary layer possibly due to some residual mixing. At 24:00 LT, the layer was already well developed, showing a height of 170 m with an inversion intensity of 2.3 K between the surface and the top of the inversion (Table 4.3). With nocturnal radiative cooling, this layer deepened with time, reaching heights of 200 m at 04:00 LT and 300 m at 06:00 LT. In this evolution, the thermal discontinuity also increased from 2.53 K at 04:00 LT to 3.9 K at 06:00 LT.

Table 4.3: Values of the height of the boundary layer (h_s), of the virtual potential temperature at the top of the layer ($\theta_v(h_s)$), and of the thermal inversion discontinuity ($\Delta\theta_v$) under nocturnal conditions during the NE-TBLE.

Local Time	hs (m)	θ_v (hs) (K)	$\Delta\theta_v$ (K)
20:00	Not clear		
24:00	170	302.503	2.336
04:00	200	301.333	2.533
06:00	300	301.666	3.933

The virtual potential temperature at the top of the nocturnal boundary layer decreased from 302.5 K at 24:00 LT to 301.3 K at 5:00 LT. During this period, the major cooling occurred with a rate of -0.29 K/h. After this time, the NBL was nearly quasi-steady between the hours of 04:00 and 06:00 LT (during which times no significant cooling was observed).

The intensity of the inversion layer at 06:00 LT was calculated as 13.11 K/km. Figure 4.7 displays the evolution of the NBL during the NE-TBLE. The NBL observed was shallow. The NBL evolved during a period of calm wind and hence its development is strongly related to the strength of radiative cooling at the surface. Its

evolution depends largely on the conditions under which it was initiated (at sunset). The NBL also has a slow evolution time scale of 10 hours (Nieuwstad & Tennekes, 1981; Nobre *et al.*, 1996). In the tropics, due to the lower Coriolis forcing, the time scale of the evolution would be even longer. This time scale makes the evolution of the NBL less sensitive to surface forcing in comparison to the evolution of the CBL that showed a rapid response to surface forcing in the early morning period between 08:00 LT and 12:00 LT.

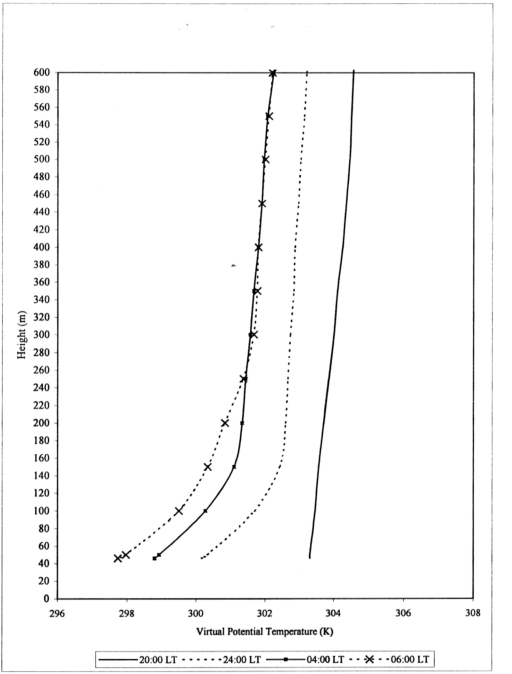

Figure 4.7: Time evolution of the nocturnal boundary layer (NBL) during the NE-TBLE (24^{th}-30^{th} January 2000).

4.3.2 Tropical Boundary Layer Experiment During The South-West Monsoon (SW-TBLE)

The observations of the SW-TBLE, which were carried out during September (11^{th} to 14^{th} 2000), are presented in this section. Similar to the NE-TBLE, using a slow rise radiosonde ascent of about 3 m/s, a four-hourly observations schedule was made during the afternoons and an intensive two-hourly ascent schedule during the mornings. Sondes were launched at a 4:00, (6:00), 8:00, (10:00), 12:00, 16:00, 20:00, and 24:00 local time (LT), where times in parentheses indicate extra soundings.

The tropical ABL was analysed using the radiosonde measurements to characterise the daytime and nocturnal evolution of the CBL during the SW monsoon. Using a four-day data set, a mean approach utilising virtual potential temperature during convective and stable conditions is described below.

4.3.2.1 SW-TBLE Micrometeorological Description

The micrometeorological conditions at the surface during the experiment at the site were again obtained from the MMS. The global solar radiation behaviour is shown in Figure 4.8a. The diurnal patterns during the whole period were essentially identical. The variations of dry and wet bulb temperatures are displayed in Figure 4.8b, where a maximum temperature with a well characterised diurnal cycle is shown. Minimum values were observed on September 14^{th}. The behaviour of air and wet bulb temperatures is presented in Figure 4.8b, with the maximum temperature reaching above 33 °C in the afternoon (12:00 to 14:00 LT). The wind speed, shown in Figure 4.8c, clearly shows a diurnal cycle with values ranging up to 4 m/sec (at maximum

thermal turbulence time) and being negligible (lower than 0.5 m/sec) during the nocturnal period. The predominant wind is from the south quadrant, with short periods of wind from the east (Figure 4.8d).

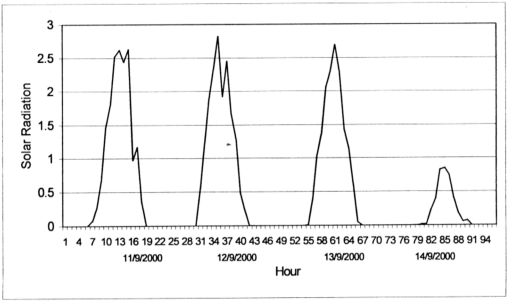

Figure 4.8 a: Time series of the hourly values of solar radiation during the SW-TBLE.

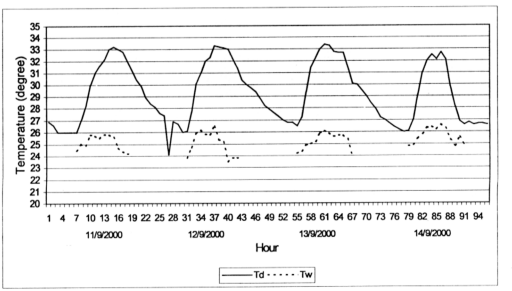

Figure 4.8 b: Time series of the hourly values of dry and wet bulb temperature (^{O}C) during the SW-TBLE.

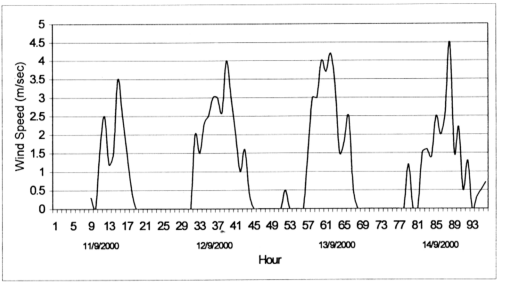

Figure 4.8 c: Time series of the hourly values of wind speed during the SW-TBLE.

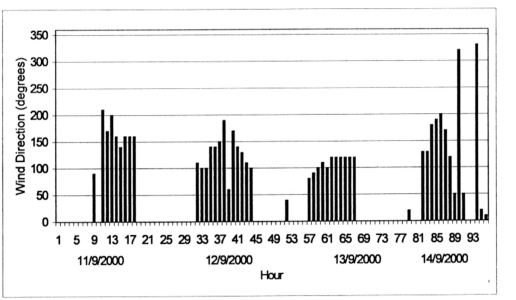

Figure 4.8 d: Time series of the hourly values of wind direction during the SW-TBLE.

4.3.2.2 Convective Boundary Layer Evolution during the SW-TBLE

As in the case of NE-TBLE, the determination of the CBL height and of its respective parameters was made using the following procedure. For all the days, individual profiles of the virtual potential temperature (θ_v) were determined and linearly interpolated at 50 m intervals. These profiles were grouped as a function of hours and the mean profile was then calculated. In this way, a typical mean composite profile was obtained as a function of local time. From this composite profile, the growth and heating rates were estimated using similar analyses to those employed for the results of the NE monsoon CBL as detailed further above.

The observations of the boundary layer were obtained by radiosondings at times of 8:00, 10:00, 12:00, and 16:00 LT. Individual profiles of the virtual potential temperature (θ_v) were determined and linearly interpolated at 50 m intervals. The 10:00 LT composite profile was calculated with two soundings while the profiles for the remaining times were performed with four soundings.

Presented in Table 4.4 are values of the diurnal evolution of the convective boundary layer height (h_c), the mean virtual potential temperature (θ_v) of the mixing layer, and the gradient of virtual potential temperature above the CBL top (γ_θ), during a clear day. During the day, the ABL height in the tropics began with a 300 m depth at 8:00 LT, increasing to 700 m by about 10:00 LT with a growth rate of 200 m/h. After this, the layer reached a height of 1200 m at midday (12:00 LT) with a higher growth rate of 250 m/h. Later in the afternoon, the layer was already developed and well mixed showing its highest value of the day of 1900 m at 16:00

LT. Its growth rate was 175 m/h at this time. Figures 4.9a-d show the vertical profiles of the virtual temperature at 8:00, 10:00, 12:00,, and 16:00 LT, respectively.

Table 4.4: Values of the height of the boundary layer (h_c), of the mean virtual potential temperature (θ_v) of the CBL, and of the gradient of virtual potential temperature above the top of the CBL (γ_θ) for diurnal conditions observed on clear days during the SW-TBLE.

Local Time	**CBL height (m)**	θ_v **(K)**	γ_θ **(K/km)**
8:00	300	301.36	4.01
10:00	700	305.23	3.66
12:00	1200	305.94	4.10
16:00	1900	308	4.17

The behaviour of the layer mean temperature is shown to be coherent with the diurnal cycle. It began with a value of 301.36 K (28.21 °C) and reached a maximum temperature of 308 K (34.85 °C) at 16:00 LT (Table 4.4). The heating rate was higher in the early part of the morning (1.9 K/h) during which the surface heating was eroding the stable nocturnal layer. There was a subsequent period of slow heating of 0.36 K/h until midday. The heating rate then stabilised to 0.52 K/h between 12:00 and 16:00 LT. The virtual potential temperature gradient above the inversion (the CBL top) showed a slight time variation, beginning with 4.01 K/km at 8:00 and increasing to 4.17 K/km at 16:00 LT (Table 4.4).

During the afternoon, when the surface sensible heat flux normally begins to decrease, the layer as a whole maintains (or slowly increases) its temperature. This is due to the role of the entrainment fluxes that incorporate drier and warmer air above the inversion. The entrained flux is of the same order of magnitude as the surface heat flux, which can be evaluated by doing a simple estimation with the energy

conservation equation in the layer (Fisch, 1996). The entrainment is a very important term in the estimation of the CBL growth models and it will be investigated in a subsequent chapter of this thesis.

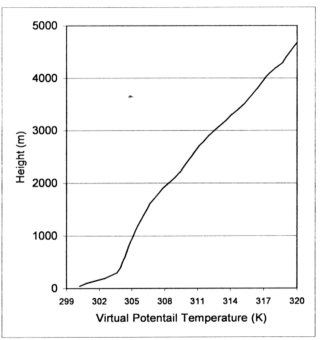

Figure 4.9 a: Composite vertical profile of the virtual potential temperature at 8:00 LT (SW-TBLE).

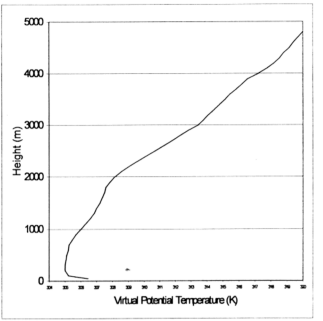

Figure 4.9 b: Composite vertical profile of the virtual potential temperature at 10:00 LT (SW-TBLE).

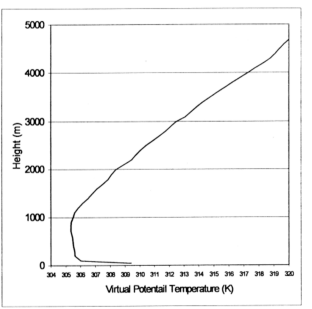

Figure 4.9 c: Composite vertical profile of the virtual potential temperature at 12:00 LT (SW-TBLE).

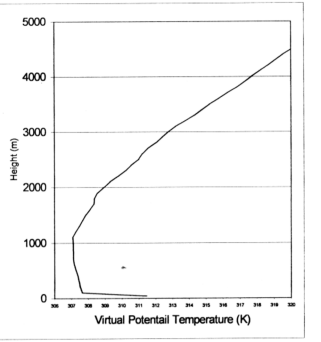

Figure 4.9 d: Composite vertical profile of the virtual potential temperature at 16:00 LT (SW-TBLE).

4.3.2.3 The Nocturnal Boundary Layer Evolution during the SW-TBLE

To characterise the nocturnal boundary layer evolution during the SW-TBLE experiment, radiosonde ascents were performed at 20:00, 24:00, 04:00, and 06:00 LT during the four days of the experiment.

The procedures adopted for the determination of the characteristics of the NBL were similar to that used for the NE-TBLE experiment. The profiles were interpolated at every 50 m and grouped as a function of hours. A mean profile was subsequently calculated for each time and the mean characteristics determined as a function of this profile. The profiles of 20:00, 24:00, and 04:00 were calculated with 4 releases while the 06:00 profile was calculated with 2 releases only.

In the following analysis, the thermal discontinuity (K), is defined as the difference between the virtual potential temperatures at the top of the nocturnal boundary layer and at the surface respectively. The intensity of the thermal inversion (K/km) is defined as the thermal discontinuity divided by the thickness of the layer. The layer cooling rate (K/h) is the temporal variation in the virtual potential temperature at the top of the NBL.

Table 4.5 presents values of the nocturnal evolution of the height of the boundary layer top (h_s), the virtual potential temperature (θ_v (h_s)) at the top of the layer, and the thermal inversion discontinuity ($\Delta\theta_v$) for the SW-TBLE. At the 20:00 LT ascent, the nocturnal boundary layer lay at a height of 150 m, with a virtual potential temperature at the top of 304.95 K. The NBL height increased to 300 m (at 24:00 LT), 400 m (at 04:00 LT), and reached a final height of 550 m at 06:00 LT.

During this period, the thermal discontinuity intensified from 0.7 K (at 20:00 LT) to 3.7 K (at 06:00 LT), whereas the layer cooled between 20:00 LT and 24:00 LT at a rate of -0.14 K/h. The layer became stationary after this time. To illustrate this behaviour, Figure 4.10 shows the temporal evolution of the NBL during the SW-TBLE.

Table 4.5: Values of the height of the boundary layer (h_s), of the virtual potential temperature at the top of the layer (θ_v (h_s)), and of the thermal inversion discontinuity ($\Delta\theta_v$) in nocturnal conditions during the SW-TBLE.

Local Time	**h_s (m)**	**θ_v (h_s) (K)**	**$\Delta\theta_v$ (K)**
20:00	150	304.95	0.7
24:00	300	304.4	2.45
04:00	400	304.65	3.575
06:00	550	304.75	3.7

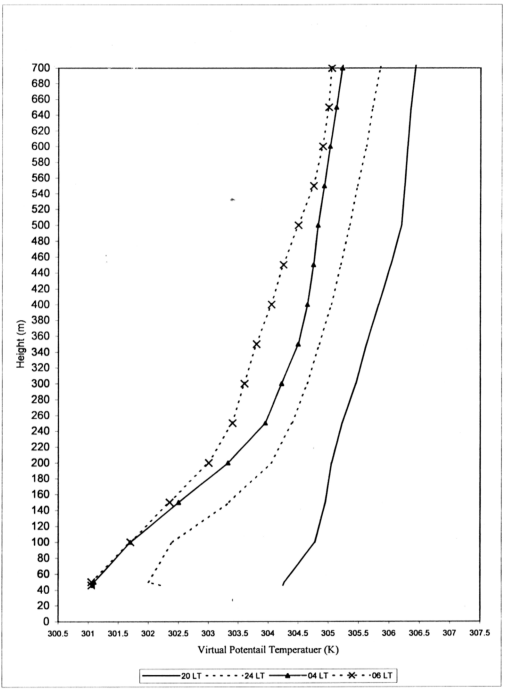

Figure 4.10: Temporal evolution of the NBL during the SW-TBLE

4.3.3 Wind-Profiles Analysis and Sea Breeze circulation During the TBLEs

The structure and the evolution of the atmosphere is still a subject of many research activities in meteorological literature. The different studies can be put into different categories, according to the data available and the method used.

Due to the fact that the atmosphere is an interaction between the thermodynamics and the dynamics of the atmosphere, it is seen that we should present a brief discussion on the possible role of sea–breeze on the evolution of the boundary layer in the tropics. As an important factor in the transfer of heat energy from the earth's surface to the atmosphere, the sea breeze circulation has a role in the boundary layer's evolution (Abu Samah & Tick, 1992). This would complete our discussion on the observational aspects presented in the previous sections.

The Sea Breeze: review

The sea breeze is a quasi-regular circulation that develops due to the differential heating of the air over land and over sea. As the sun heats the boundary layer over land, the resulting pressure gradient causes the movement of low-level air from sea to land (sea breeze) with a return flow aloft (return current). The existence and the intensity of the sea breeze depend strongly on seasonal and latitudinal factors as well as on the time of the day. On cooler regions of the globe, the sea breeze is a common feature during spring and summer, when the temperature difference between land and sea is at its maximum, whereas, it is a regular phenomenon throughout the year on many tropical and subtropical coastal regions.

Normally, the sea breeze starts in the morning, a few hours after sunrise, when the solar radiation starts heating the boundary layer over land. In the afternoon, when the boundary layer heating over land is at its maximum, the sea breeze is most intensive. If the large-scale flow is weak, the direction of sea breeze often veers with time. This is a result of the Coriolis force having an impact on the air current. Later in the evening, as the solar radiation decreases, the sea breeze and its associated cloudiness die out.

The land and sea breeze are still the interest of many articles found in the meteorological literature both theoretical and observational studies (Tijm *et al.*, 1999). The observational studies always depend strongly on the available measuring equipments. Due to the lack of good instruments, the first sea breeze studies consisted mainly of observing how far the sea breeze reached inland (Simpson, 1994). Later, sea breeze have been observed with the help of aircraft (Kraus *et al.* 1, 1990; Frinkele *et al.*, 1995) and remote sensing techniques such as pulsed Doppler lidar (Banta *et al.*, 1993; Banta, 1995) and Dual Doppler radar (Laird *et al.*, 1995). Theoretical studies can be split into the analytical and the numerical studies. The studies performed by Rontunno (1983), and Dalu and Pielke (1989) are an example of the analytical sort. One of the first three-dimensional studies was performed by Pielke (1974), whereas Bechtold *et al* (1991) and Arritt (1993) use two-dimensional models to study sea breezes under a wide range of conditions (i.e., large-scale winds, stability). A study which involved nonhydrostatic models with which the turbulent properties of sea breezes were presented by Koo and Reible (1995) and Kelvin-Helmholtz instabilities in gravity currents by Xu *et al.* (1996). The study by Tijm *et al.* (1999) investigated the sea breeze in the Netherlands. They used data from a wind

profiler in the investigation of the vertical structure of the sea breeze with the accompanying return currents at the North Sea coast. The sea breeze and as well as the return current of their observation were simulated well by a simple two-dimensional mesoscale model. Their study is an example of the sea breeze structure in the midlatitude region.

The previous studies have provided insight into the origin and development of the sea breeze. In the tropics, the land and sea breeze were addressed as major processes in the boundary layer structure especially the surface layer. Further, its role in the dispersion of pollutants was always addressed in the literature. For example, Sham *et al.* (1991) showed that the boundary layer is very much influenced by the land and sea breezes during the haze episode. In view of its importance, Abu Samah and Lim (1992) included the circulation into the urban pollution model. Their investigation on the meteorological conditions associated with air pollution in the Klang Valley, Malaysia indicates clearly the importance of the land and sea breeze circulation in influencing the diurnal concentration of air pollution. The influence was investigated using ATDL model. Incorporating the sea-land breeze circulation in the model enabled the simulation of the observed variation accurately.

Theoretically, the sea-land breeze circulation was included into the urban pollution model. Consider a two grid squares in which one of them contains an area source of pollution and the other containing the receptor at its centre then the pollution concentration (C_A) due to the area source Q is given by Equation (4) (Abu Samah & Lim, 1992).

$$C_A = \sqrt{\frac{2}{\pi}} \frac{Q}{Ua(1-b)} \sum_{i}^{N} Q_i \left[x_{2i}^{1-b} - x_1^{1-b} \right] \qquad (4)$$

Assuming N area sources located upwind of the receptor, Equation (4) gives the concentration of the air pollutants at any given time due to all theses sources. U is the mean wind speed, x the distance from the area source and *a, b* are the stability parameters. Hanna (1972) recommended the values of $a = 0.4$ and $b = 0.91$ for a sunny day (unstable), $a = 0.15$ and $b = 0.75$ for cloudy day (near neutral), and $a = 0.06$ and $b = 0.71$ at night (stable).

Given U as the mean wind speed, Equation (4) was modified by substituting U with U (t) based on the analytical model of the sea and land breeze in the equatorial region as derived in Lim (1979),

$$U(t) = \sqrt{u(t)^2 + v(t)^2}$$

u(t) and *v(t)* given as,

$$u(t) = u_s + \sum_{i=1}^{2} M_i \sin(\Omega_i t - \phi_i + \psi_i)$$

with $\tan \psi_i = \frac{k}{\Omega_i}$ and $M_i = \frac{A_i}{\sqrt{k^2 + \Omega_i^2}}$, and

$$v(t) = v_s \sum_{i=1}^{2} N_i \cos(\Omega_i t - \phi_i + \psi_i)$$

with $tan\ \psi_i = \frac{k}{\Omega_i}$ and $N_i = \frac{A_i f}{\sqrt{k^2 + \Omega_i^2}}$, where u_s is the zonal component of the synoptic wind, v_s is the meridional component of the synoptic wind, f is the coriolis parameter, k is the coefficient of resistance, A_i and ϕ_i are constants determined from the first two harmonics of a Fourier series used to approximate a specified land-sea breeze temperature difference and $\Omega_1 = 2\Omega_2 = 7.3 \times 10^{-5} s^{-1}$. Lim found that the value of k influences the diurnal shift and rotation rate of the local wind direction. Based on physical arguments, he showed that an appropriate value of k for the costal region was found to have a value of $9.4 \times 10^{-5} s^{-1}$.

Wind – Profiles description

A case study from each of the TBLEs, is considered to illustrate the interaction between the convection, sea breeze and the synoptic winds in the tropical boundary layer. An investigation of the sea breeze circulation and its characteristic are presented. The inclusion of the sea-breeze analysis enhances our understanding of the boundary layer growth in general and the sea breeze in particular.

Two data sets of the wind-profiles during the TBLEs were considered for the analysis, i.e., January 27th, 2000 (NE-TBLE) and September 11th, 2000 (SW-TBLE). The vertical profiles of wind speed, wind direction and the wind components; the zonal (u) & meridional (v), were calculated from the radiosondes ascents at different times during the day.

Considering the NE case study, the vertical profile of the wind speed, wind direction and wind components are shown, at different times of the day, in Figures 4.11A, 4.11B and 4.11C, respectively. To have a clear picture of the wind dynamics, the time height plot of the winds is also presented (Figure 4.12).

From the vertical-profiles in Figures 4.11, the prevailing wind is NE (both u and v negative). Then the inflow sea breeze is seen near the ground as an almost calm region (1-2 m/s). Above the sea breeze there is a very deep layer - up to 3 km with rather strong NE winds, the wind decreases further up.

The wind speeds are very low in the area. Due to the increasing differences between the air temperature over land and over the sea, the sea breeze starts to form after sunrise. In V time height-plot in Figure 4.12, the sea breeze starts at 10:00 LT and persists until 13:00 LT. The intensity and extent of the sea breeze increase with time until it is switched off. Its influence is felt in the lower atmosphere up to 700 m above the surface. It is also observed that the sea breeze still present in the afternoon hours (15:00 to 18:00 LT) but with lower levels (500 m). An important observation would be the existence of the sea breeze wind during the nighttime. The wind did not mix with the air above and stayed in the lower level.

It is interesting to note that the sea breeze is switched off by the strong synoptic wind at midday. The convection processes are maximum at this time, an entrainment quickly brings easterly momentum to the surface and suppresses the sea

breeze signature in the surface layer. The sea breeze signature starts to appear again in the afternoon hours only when the convection processes are weakened. These observations are confirmed by the wind direction analysis in Figure 4.11B where the winds near to the ground are southerly, changing direction when the synoptic winds dominates. The wind direction has also changed in the late afternoon hours where the sea breeze is felt again.

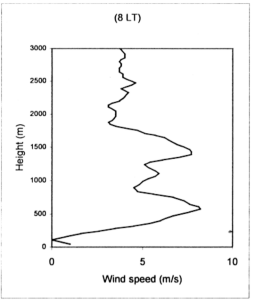
(8 LT)
Height (m)
3000
2500
2000
1500
1000
500
0
0
5
10
Wind speed (m/s)

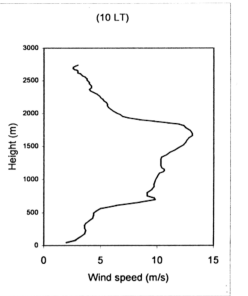
(10 LT)
Height (m)
3000
2500
2000
1500
1000
500
0
0
5
10
15
Wind speed (m/s)

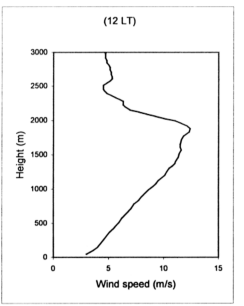
(12 LT)
Height (m)
3000
2500
2000
1500
1000
500
0
0
5
10
15
Wind speed (m/s)

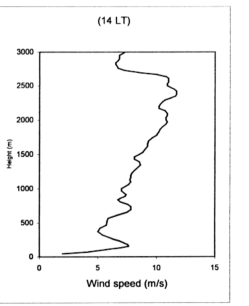
(14 LT)
Height (m)
3000
2500
2000
1500
1000
500
0
0
5
10
15
Wind speed (m/s)

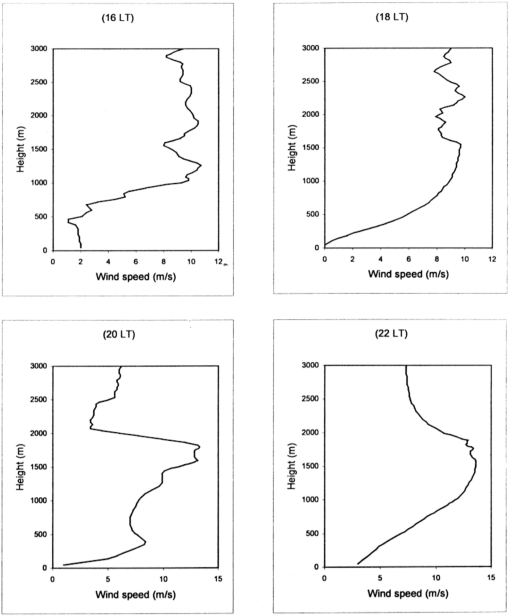

Figure 4.11 A: Vertical profiles of the wind speed, at 8, 10, 12, 14, 16, 18, 20 7 22 LT, on the 27th January 2000

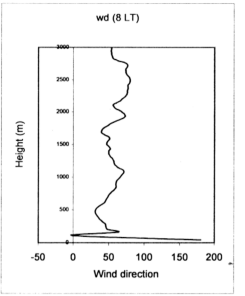
wd (8 LT)
Height (m)
3000
2500
2000
1500
1000
500
0
-50
0
50
100
150
200
Wind direction

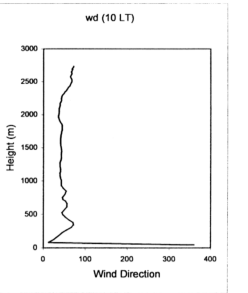
wd (10 LT)
Height (m)
3000
2500
2000
1500
1000
500
0
0
100
200
300
400
Wind Direction

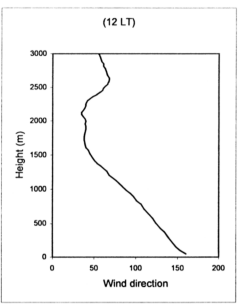
(12 LT)
Height (m)
3000
2500
2000
1500
1000
500
0
0
50
100
150
200
Wind direction

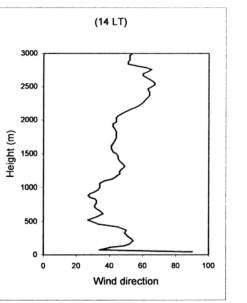
(14 LT)
Height (m)
3000
2500
2000
1500
1000
500
0
0
20
40
60
80
100
Wind direction

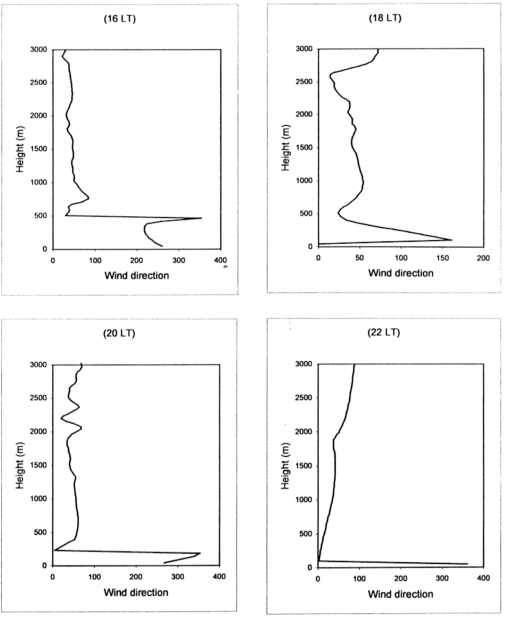

Figure 4.11 B: Vertical profiles of the wind direction, at 8, 10, 12, 14, 16, 18, 20 7 22 LT, on the 27th January 2000

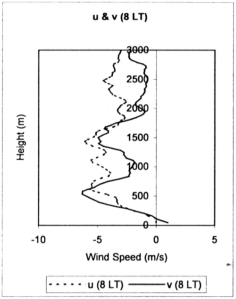
u & v (8 LT)
Height (m)
3000
2500
2000
1500
1000
500
0
-10
-5
0
5
Wind Speed (m/s)
u (8 LT)
v (8 LT)

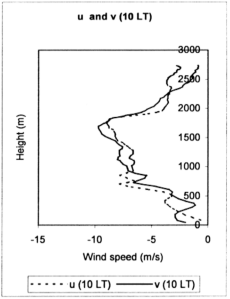
u and v (10 LT)
Height (m)
3000
2500
2000
1500
1000
500
0
-15
-10
-5
0
Wind speed (m/s)
u (10 LT)
v (10 LT)

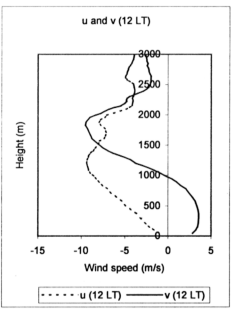
u and v (12 LT)
Height (m)
3000
2500
2000
1500
1000
500
0
-15
-10
-5
0
5
Wind speed (m/s)
u (12 LT)
v (12 LT)

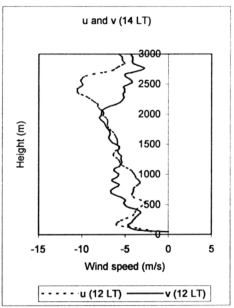
u and v (14 LT)
Height (m)
3000
2500
2000
1500
1000
500
0
-15
-10
-5
0
5
Wind speed (m/s)
u (12 LT)
v (12 LT)

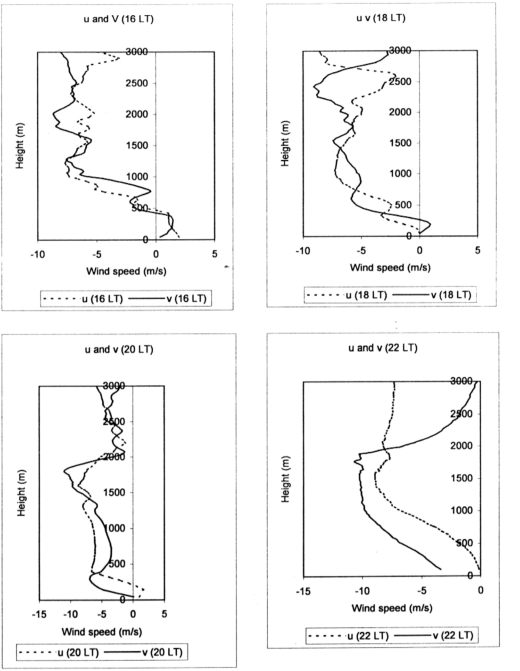

Figure 4.11 C: Vertical profiles of the wind components (u & v), at 8, 10, 12, 14, 16, 18, 20 & 22 LT, on the 27th January 2000

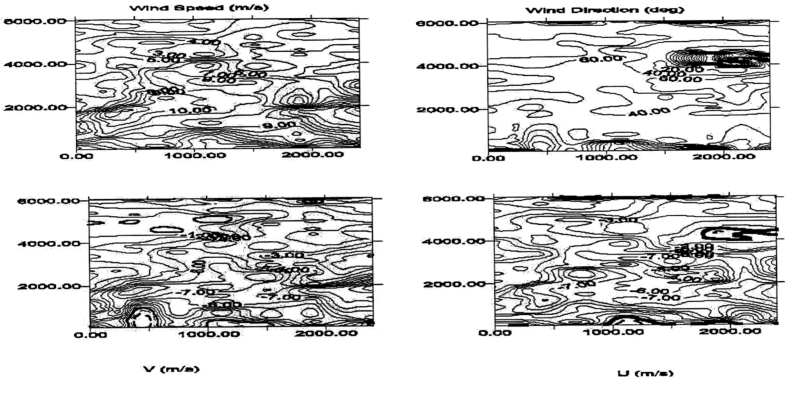

Figure 4.12: Raw wind analysis on the 26th, January 2000.

The wind profile analysis during the SW-TBLE is shown in Figures 4.13. The vertical profile of the wind speed, wind direction and wind components presented in Figures 4.13 A, 4.13 B and 4.13 C, respectively. The radiosondes ascents were done at 8, 12, 16 & 20 LT.

During this time of the year, wind in the tropical lower troposphere is basically southwesterly with a typical speed of 2-5 $m.s^{-1}$. Aloft is the equatorial easterly with a typical speed of 10-15 $m.s^{-1}$. The low level southwesterly transverse the mountain barrier of Sumatra and hence the west coast of the Peninsular Malaysia becomes a rain shadow area due to the subsidence of the southwesterly (Abu Samah & Lim, 1992). This is illustrated in Figures (4.13 A and 4.13 B).

To investigate the sea breeze circulation during the monsoon, the time height of the wind speed, direction and wind components for the 11th, September 2000 is presented in Figures 4.13 C and 4.14.

Eventhough the two monsoons have the same evolution time period, 10:00 –12:00 LT, a deeper growth is experienced during the SW. A height of 1000m is seen in the midday in Figure 4.14 (v time height plot). This deeper growth is due to the fact that synoptic winds and the sea breeze have the same direction and hence the sea-breeze circulation is enhanced.

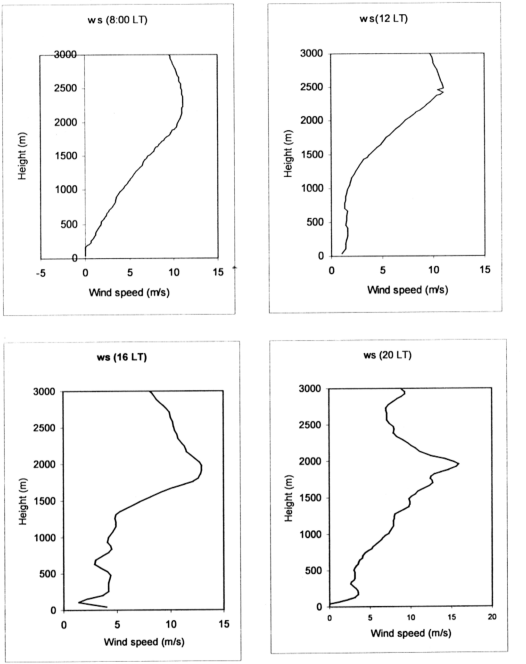

Figure 4.13 A: Vertical profiles of the wind speed at 8, 12, 16 & 20 LT, on the 11th September 2000.

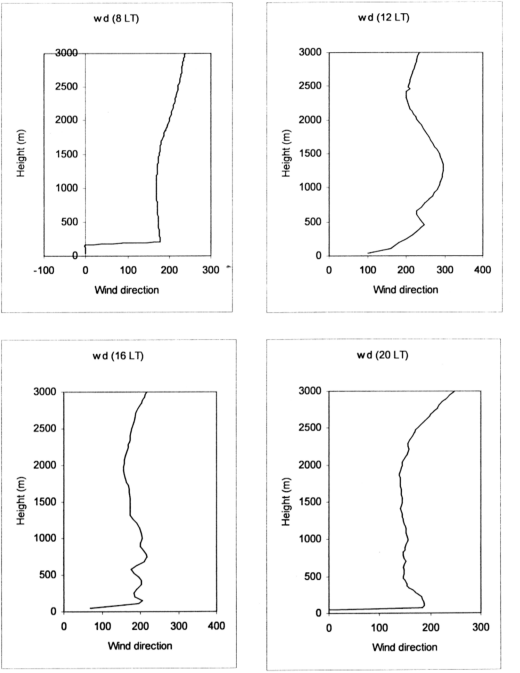

Figure 4.13 B: Vertical profiles of the wind direction at 8, 12, 16 & 20 LT, on the 11th September 2000.

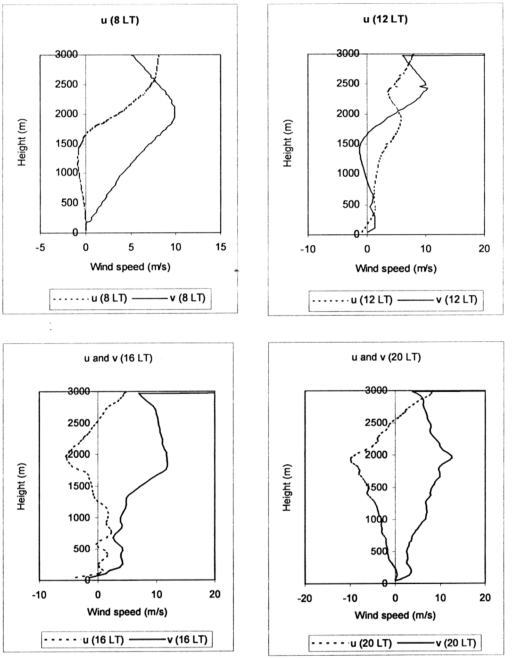

Figure 4.13 C: Vertical profiles of the wind components at 8, 12, 16 & 20 LT, on the 11th September 2000.

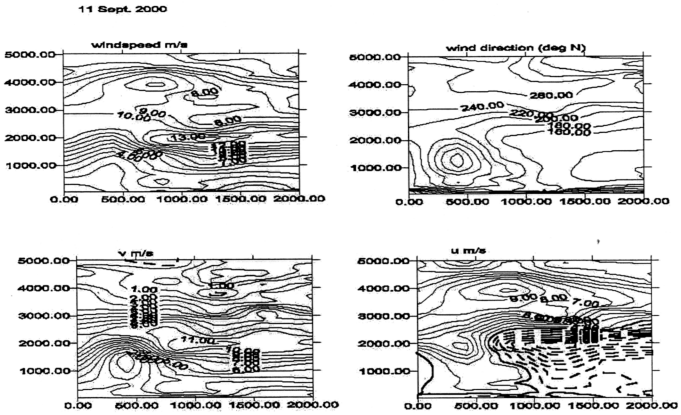

Figure 4.14: Dynamic Flux on the 11th, September 2000.

mmary Discussion on the wind analysis

om our discussion, the above-presented equations illustrated the contribution and the portance of the wind components in the growth and the mixing processes in the pical atmospheric boundary layer. The homogeneity of the boundary layer assumption, ich is widely used, is inaccurate. Therefore, two or three-dimensional model would lude the contribution and role played by the sea-breeze circulation in the growth and dispersion generally.

The observed pattern, in Figure 4.12, is quite different from that in Athens eece). In Athens the conditions that favor the development of the sea-breeze during summer is Southwesterly winds (coming from northeast and blowing towards thwest), the name of the wind is Etesian. However in Athens the sea breeze near the und is rather strong - typically 5 m/s - and the return flow above the sea breeze near ground is very weak - typically 1-2 m/s (and in the opposite direction). We observe absolute opposite in our measurements - a weak breeze near the ground and a strong deep wind above the calm region (Gryning, personal communication). Therefore the erved sea breeze is not a typical "European" sea breeze. Other effects might be uencing the development of the sea breeze in Malaysia.

Figure 4.11 C shows an interesting feature of the tropical boundary layer npared to its midlatitude counterpart. The wind components (u and v) showed a form vertical profile in the midlatitudes, where the contrast is observed in our

alysis. Only a similar uniform distribution was observed at 14:00 LT profile up to the ight of the formed mixed-layer. This is due to the intense convection of the tropical undary layer at this time of the day. Further difference is the non-existence of the ernal boundary layer in the tropics. This is attributed to the strong convection that ads to mix the sea breeze fast offsetting its signature.

In summary, the vertical structure of the sea breeze over the study area has the lowing characteristics:

- The sea breeze at noon occupies a layer of the order of 600 – 1000 m depending on the season.
- The influence of the sea breeze extends higher during the SW monsoon compared to that during the NE monsoon. This is due to the favourable synoptic wind direction that enhances the sea breeze.
- The temperature field does not reflect the expected cooling as a sign of sea breeze passage.
- The sea breeze circulation is influenced by the synoptic forcings during the different periods of its development.

To conform more to the general objective of the thesis, our discussion in the next apters, will be centered on the investigation of the conventional slab models and its ility to simulate the evolution and the structure of the daytime boundary layer in the pics. The slab model is a thermodynamic 1-D model and as such it assumes a rizontal homogeneity of the atmosphere and therefore, does not include a possible

uence of the sea-breeze circulation. Though, the dynamics of the boundary layer will be discussed further. Acknowledging the subject importance in enhancing our lerstanding of the boundary layer, this would be neglected in the mean time and would considered as extension of the present work.

SUMMARY AND DISCUSSION

studying the evolution of the convective and nocturnal boundary layers in the humid pical area, some insights can be gained from analysing and comparing the observed files obtained from the NE-TBLE and the SW-TBLE (see Figure 4.15).

The observations during the NE-TBLE showed that the mixing layer mean perature was slightly warmer (with higher heating rates) in clear conditions compared h temperatures during cloudy conditions. The influence of the surface through sensible t flux is important but was not the only effect; the influence of entrainment was shown contribute to maintaining the mixed layer's temperature and to the development of the L height in the afternoon.

Heating rate became stationary in the afternoon. In spite of the reduced surface ting in the late afternoon, the layer was still warmed by the entrainment flux of hot l dry air from above the CBL. This is found to be very similar to the behaviour of the nazon convective boundary layer (Fisch *et al.*, 1996).

Compared to observations during the SW-TBLE, the CBL grew slightly stronger ring the NE-TBLE. The final mixing layer height was 150 m deeper compared to the ght observed during the SW-TBLE. This can be attributed to the higher growth rate in morning during the NE-TBLE (375 m/h versus 225 m/h for the NE-TBLE and SW-BLE respectively, during the period 8:00-12:00 LT). During both experiments, the ating rate in the afternoon was less than 0.5 K/h.

Due to the calm wind at night, the nocturnal boundary layer in the tropics is allow. This reduces the influence of mechanical turbulence and hence vertical diffusion nnot deepen the nocturnal layer. Due to these calm conditions at night, the NBL was allower during the NE-TBLE than the equivalent layer during the SW-TBLE. The eater depth of the NBL during the SW-TBLE may be due to the influence of the echanical turbulence. The observed NBL during the SW-TBLE was similar to the NBL served over the forest site in the Amazon boundary layer (Fisch, 1996).

Generally, a perfectly clear day is difficult to obtain since clouds in the humid pics are dominant and tend to occur almost all the time. Therefore, the cloud cover ll, to an extent, affect the surface fluxes that control the boundary layer growth. ecause clear conditions were seldom experienced in this case, it is very likely that the easurement of mixing height to 2700 m (on the 27th January) could be an outlier aused by a very strong updraft of short duration and which was not representative of neral conditions). This conclusion is supported by the fact that such similar servations were not found in any of the other 3 clear days of the NE monsoon or during

dry period of the SW monsoon. Besides, the mixing height returned to a value of 0 m for that day which is similar to the usual values in this region. The hourly perature on 27th January was high from the early morning onwards and so was the r radiation (Figures 4.4a and 4.4b).

With respect to the gradient of virtual potential temperature above the CBL (γ_θ), eral authors in the literature have considered the temperature gradient above the vective boundary layer to be time-invariant (e.g., Tennekes, 1973; Driedonks, 1982). wever, in this study, this slope has a small dependence, slowly increasing with time: n 4.3 K/km (at 8:00 LT) it increased to 5.3 K/km (at 16:00 LT) during the NE-TBLE, from 4.01 K/km (at 8:00 LT) to 4.17 K/km (at 16:00 LT) during the SW-TBLE. 'γ_θ' s observed to increase with time at the TBLE site, attaining slightly higher values npared to those observed in the Amazon boundary layer over forest, where a slow ease from 1.8 K/km to 3.3 K/km was reported by Nobre *et al.* (1996). Of particular erest is that the clear-day data set at the TBLE site reveals temporal variations in the dient of virtual potential temperature above the CBL from 3.8 K/km to 7.6 K/km. ese values are similar to the values observed over the pasture site (3.6 K/km to 8.0 km in RBLE-II) as reported by Nobre *et al.* (1996).

Compared to the CBL and NBL heights under different weather conditions, the final nvective boundary layer height was higher than values reported for mid-latitude ions. Using data on the evolution of the daytime boundary layer at Cabauw, the

etherlands, Driedonks (1982) observed a mixing-height of between 900-1350 m for the BL.

Compared with the Amazonian mixing layer observations, the CBL heights in our site e similar to those observed over the Amazonian pasture areas (RBLE-II) (Nobre *et al.*, 96; Fisch *et al.*, 1996; Fisch *et al.*, 1996). The CBL height typically reaches a height of ore than 2 km in the afternoon.

Compared to observations of an equatorial rain forest in the ABLE 2A experiment Iartin *et al.*, 1988), the CBL at the TBLE site was observed to grow deeper. During the ry" season in central Amazon, the maximum depth of the mean mixing layer reached a ight of 1200 m at 13:00 LT, while the maximum depth grew above 2000 m at the BLE site. However the maximum CBL height observed during the Land Surface ocesses Experiment (LASPEX-97, an experiment conducted at Anand, a semi-arid tion in the Sabarmati basin of Gujarat), reached 3.2-3.6 km under hot weather nditions (Nagar *et al.*, 2001). This could be due to the greater amount of surface heat xes in that region compared with the TBLE site.

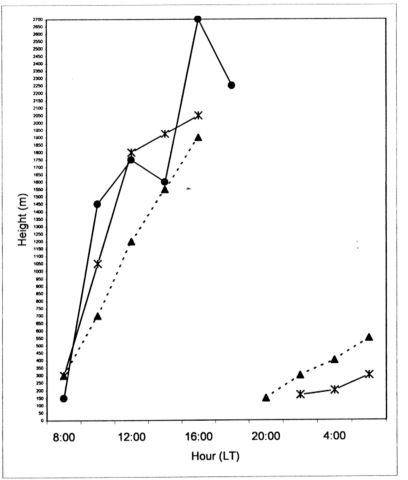

gure 4.15: Schematic diagram of the ABL based on observed data during the NE-BLE (., h during clear conditions; *, h during cloudy conditions) and the SW-TBLE).